Materials & Design 185 (2020) 108256

Contents lists available at ScienceDirect

Materials & Design

journal homepage: www.elsevier.com/locate/matdes

Ordered micropillar array gold electrode increases electrochemical signature of early biofilm attachment

Solange E. Astorga [a, e], Liang Xing Hu [b], Enrico Marsili [c, d, e, **], Yizhong Huang [a, *]

[a] School of Material Science and Engineering, Nanyang Technological University, 639977, Singapore
[b] School of Mechanical and Aerospace Engineering, Nanyang Technological University, 639798, Singapore
[c] Department of Chemical and Materials Engineering, Nazarbayev University, 010000, Nur-Sultan, Kazakhstan
[d] Environment & Resource Efficiency Cluster (EREC), Nazarbayev University, 010000, Nur-Sultan, Kazakhstan
[e] Singapore Centre for Environmental Life Sciences Engineering (SCELSE), Nanyang Technological University, 637551, Singapore

HIGHLIGHTS

- Electrochemical signature of *E. coli* early biofilm was measured on microstructured electrodes.
- Microstructured electrodes enhanced early biofilm attachment.
- Microstructured electrodes increased EET rate and detection of early biofilms by 22%.
- Biofilm formation decreased interfacial resistance via impedance spectroscopy.
- Electronic and confocal microscopy confirm that biofilm forms near electrode microstructures.

GRAPHICAL ABSTRACT

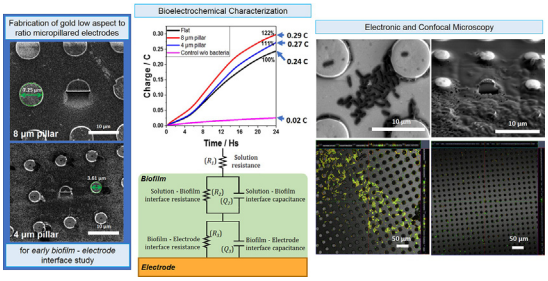

ARTICLE INFO

Article history:
Received 27 May 2019
Received in revised form
4 October 2019
Accepted 4 October 2019
Available online 9 October 2019

Keywords:
Bioelectrochemistry
Extracellular electron transfer (EET)
Electroactive biofilm
Biofilm-surface interaction
Micropillared electrode
Surface modification

ABSTRACT

Extracellular electron transfer (EET) from microorganisms to insoluble metals and electrodes is relevant to energy recovery from wastewater, green production of high-added value chemicals, and biosensors for food, environmental, and clinical applications. Microstructured electrode surfaces increase EET rate in bioelectrochemical systems, thus enabling higher sensibility and power output as well as the detection of bacteria and biofilms in bioelectrochemical sensors. However, many aspects of the EET process, particularly in early biofilm stages, are still poorly understood. We report a microstructured gold electrode maintained at oxidative potential to support the growth of *Escherichia coli*, measure the electrochemical output, and analyze the EET rate during early biofilm formation. The charge outputs of the modified electrodes are up to 22% higher than the control electrodes, enabling the electrochemical detection of early *E. coli* biofilms. The electrode microstructures promote biofilm attachment, as confirmed by field emission scanning electron microscope (FESEM) and confocal laser scanning microscope (CLSM) imaging. Following biofilm formation, the resistance to charge transfer at the biofilm-electrode interface decreases and the capacitance increases as shown by EIS analysis. Overall, these

* Corresponding author.
** Corresponding author. Department of Chemical and Materials Engineering, Nazarbayev University, 010000, Nur-Sultan, Kazakhstan.
E-mail addresses: enrico.marsili1@gmail.com, enrico.marsili@nu.edu.kz (E. Marsili), yzhuang@ntu.edu.sg (Y. Huang).

https://doi.org/10.1016/j.matdes.2019.108256

results contribute to the understanding of EET in early biofilms, towards developing sensitive bioelectrochemical sensors for biofilm detection.

1. Introduction

Bioelectrochemical systems (BES) are relevant to the development of microbial fuel cells and biosensors for food, environmental and clinical applications [1]. BES are powered by interactions between viable bacterial cells and electrically conductive materials [2,3], and offer a potentiostat-controlled environment to investigate the biological phenomena using electrochemical methods [4]. Numerous bacterial species are capable of Extracellular Electron Transfer (EET) to electrodes maintained at a defined electrochemical potential [5,6]. EET originates from bacterial respiration processes in which microorganisms oxidize organic carbon sources and, in absence of soluble electron acceptors (e.g., oxygen or nitrates), use the electrode as a terminal electron acceptor [7,8]. EET in microorganisms is generally thought to occur through one or more of three main mechanisms: (i) direct electron transfer through transmembrane cytochrome complex [9,10], (ii) electron hopping via pili-like conductive appendages termed nanowires [11,12]; or (iii) mediated electron transfer via exogenous or microbially produced redox mediators [13,14]. In order to improve BES efficiency, it is necessary to identify the mechanisms of bacterial electron transfer into solid electrodes, yet the aforementioned EET mechanisms are not completely distinct from one another. Currently, deconvoluting them with accuracy remains a challenge [15].

Bacteria tend to accumulate at interfaces to form polymicrobial aggregates deemed biofilms [16]. Biofilms that grow on the surface of electrodes and show EET are usually termed as electrochemically active biofilms (EAB) [2,6,17]. The electron transfer diffusion is known to change as the biofilm grows [18], but an early biofilm attachment stage is sufficient to elicit a bioelectrochemical response [19]. Additionally, the electrode surface is thought to influence the early biofilm attachment [20–23], hence affecting the electrochemical performance [24], yet little research has been carried out to understand this effect. Further, the electrode material determines the current output and the biofilm attachment. Carbon electrodes have been widely used in energy-producing BES for their low-cost and biocompatibility [25]. However, they are not suitable to detect early biofilm formation, as they have high (capacitive) background current, which hinders the EET process in the early stage of bacterial colonization [26]. On the other hand, gold (Au) and Au thin film electrodes are biocompatible and have low capacitance and low electrical resistance [27,28], thus allowing sensitive EET measure [29]. Although the trend is moving away from precious metals [3], Au thin film deposition allows the systematic fabrication of electrodes with specifically designed features [30–33]. Therefore, Au electrodes represent a suitable option for biofilm and electrode-surface interaction studies.

Recent research shows that both nano- and micro-features determine the current output of biofilms [31,33,34] and that the roughness of the electrode surface contributes to the electrochemical signature and EET rate during early biofilm attachment [19]. Also, surface engineering enables the fabrication of micropillars of comparable size with bacteria, which creates a favorable platform to study the biofilm-surface interactions. Since most of the prior studies have focused on increasing the current output in BES, little attention has been given the bacteria-surface interactions in the early stage of biofilm formation. This is particularly relevant to biomedical applications, in which early detection of biofilms on devices such as catheters and prosthetic implants would allow rapid and life-saving interventions. Further, a label-free, impedance-based instrument for biofilm detection has been recently commercialized (Acea Biosciences). This device uses impedance reading at a single frequency (e.g., 10 kHz) to calculate a cell index, which is correlated to the capacitance, therefore to the concentration of bacterial biofilm. However, this approach uses only part of the information available through impedance spectroscopy [35]. Full impedance scan is preferable, in conjunction with distribution function of relaxation times (DFRT) analysis and tailored microstructured surfaces. To our best knowledge, except for our recently published work [24], this is the first study that uses DFRT analysis to characterize biofilm interactions with conductive microstructured surfaces.

Here, we report the use of an ordered micropillar array gold electrode to study the electrochemical signature of biofilm-surface interactions during early biofilm attachment. We measured the electrochemical charge, impedance, and analyzed the EET rate during early biofilm formation. The micropillared electrodes showed faster biofilm formation, as confirmed by field emission scanning electron microscope (FESEM) and confocal laser scanning microscope (CLSM) images. *Escherichia coli* biofilms were used because of their common occurrence and easy handling. *E. coli* showed low but detectable electrochemical activity in presence of the exogenous redox mediators 2-HNQ [36]. Our findings are promising towards designing electrochemical sensors that may be integrated in high-end biomedical equipment such as laparoscopes, where standard cleaning and disinfection procedures may not completely remove attached bacterial cells [37]. In fact, outbreaks due to contaminated instruments are a rare but serious concern [38]. Further, microstructured surfaces could also be employed for online biofouling/biofilm sensing in the side stream of drinking water nodes [39].

2. Experimental methods

2.1. Fabrication of Au ordered structure array electrodes

A schematic diagram of the ordered array microstructures on the electrode surface is shown in Supplementary Fig. S1. The electrodes are covered with a thin layer of Au, which is patterned into ordered arrays of cylindrical pillars with 8 μm (a) and 4 μm (b) diameter and 1 μm height (Supplementary Figs. S1a and S1b, respectively). In both cases, the distance between the centers of the pillars was 20 μm. The geometric surface of the electrode modified with 8 μm and 4 μm cylinders was 1.03 and 1.06 cm^2, with the surface of the flat electrode being 1 cm^2. Supplementary Fig. S1c is a 3D sketch of the pillar array viewed at an inclined angle. Au was selected as it is a highly conductive and biocompatible electrode material [40].

Lithography was used for fabricating the electrodes (Supplementary Fig. S2). The surface of 4-inch silicon (Si) wafer was firstly cleaned in sulfuric acid (H_2SO_4) at the temperature of 120 °C for 30 min. A 20 nm thick layer of titanium (Ti), followed by 200 nm thick layer of Au was subsequently deposited on the Si wafer surface by the magnetron sputtering system SP3 (Coaxial Power System ltd, UK). Au and Ti targets were used for the deposition process.

The chamber pressure was set at 2×10^{-2} torr, and the argon gas pressure was 3 bar. The deposition Au coating was for 1 m for Ti and 10 m for Au. The Si wafer was then covered with hexamethyldisilazane (HMDS) coating for 2 min using DELTA 150 VPO prime oven (Yields Engineering Systems, Inc, USA). HMDS is used commonly to strengthen the adhesion of the photoresist onto the surface eliminating the moisture on the wafer surface. After the wafer cooled down, a ~1.5 μm layer of photoresist (PR 7217 positive) was spin-coated on the Au surface at 5000 rpm for 30 s. Then, the photoresist was exposed to 365 nm wavelength ultraviolet (UV) light through the glass photomask for 4 s, which was followed by developing the pattern in AZ 300MIF developer solution (EMD Performance Materials Corp., USA) for 1 min. Finally, the patterned wafer was coated with a 50 nm Au layer by magnetron sputter, for 5 min, under the aforementioned chamber and argon gas pressure conditions.

2.2. Field emission scanning electron scanning (FESEM) of the bare electrodes

The surface morphology of the electrodes was characterized using FESEM 6340 (JEOL, USA) at an accelerating voltage of 30 kV and 5 kV. The FESEM images of Au ordered array electrodes with cylindrical pillars of 8 μm are shown in Fig. 1(a) (top view, magnification 3500×, 5 kV) and Fig. 1(b) (incline plane of 52°, magnification 3250×, 5 kV). Fig. 1(c) shows the thickness of the cylindrical feature is 1.30 μm height (magnification 10000×, 5 kV, tilted at 52°). The electrodes with cylindrical pillars of 4 μm diameter are shown in Fig. 1(d) (top view, magnification 3500×, 30 kV) and Fig. 1(e) (tilted 52° view, magnification 3250×, 5 kV). Fig. 1(f) shows the thickness of the cylindrical feature is 1 μm height (magnification 25000×, 5 kV, tilted at 52°).

2.3. Bioelectrochemical experiments

E. coli K12 was inoculated in Luria Bertani (LB) broth at low sodium chloride for 20 h in a shaker incubator at 200 rpm at 37 °C. Following centrifugation at 6000 rpm for 5 min at room temperature, the bacterial pellets were re-dissolved in 10 mL of MOPS 1x (3-(*N*-morpholino) propanesulfonic acid) buffer at pH = 7.4, to a final optical density at 600 nm (OD_{600}) of 0.7. The bacterial suspension was then added into the autoclave-sterilized electrochemical cell and 50 μM of 2-Hydroxy-1,4-naphthoquinone (2-HNQ) was added as redox mediator.

The electrochemical cells comprised of an 11 mL glass vial and a custom Teflon lid sealed with Parafilm layer (Bemis Company, Inc., USA). Each cell was fitted with a microstructured Au working electrode (WE) hold by a PTFE jacketed electrode holder, an Ag/AgCl reference electrode (RE) (IDA Company, China), and a Pt wire counter electrode (CE). The three electrodes were connected to a

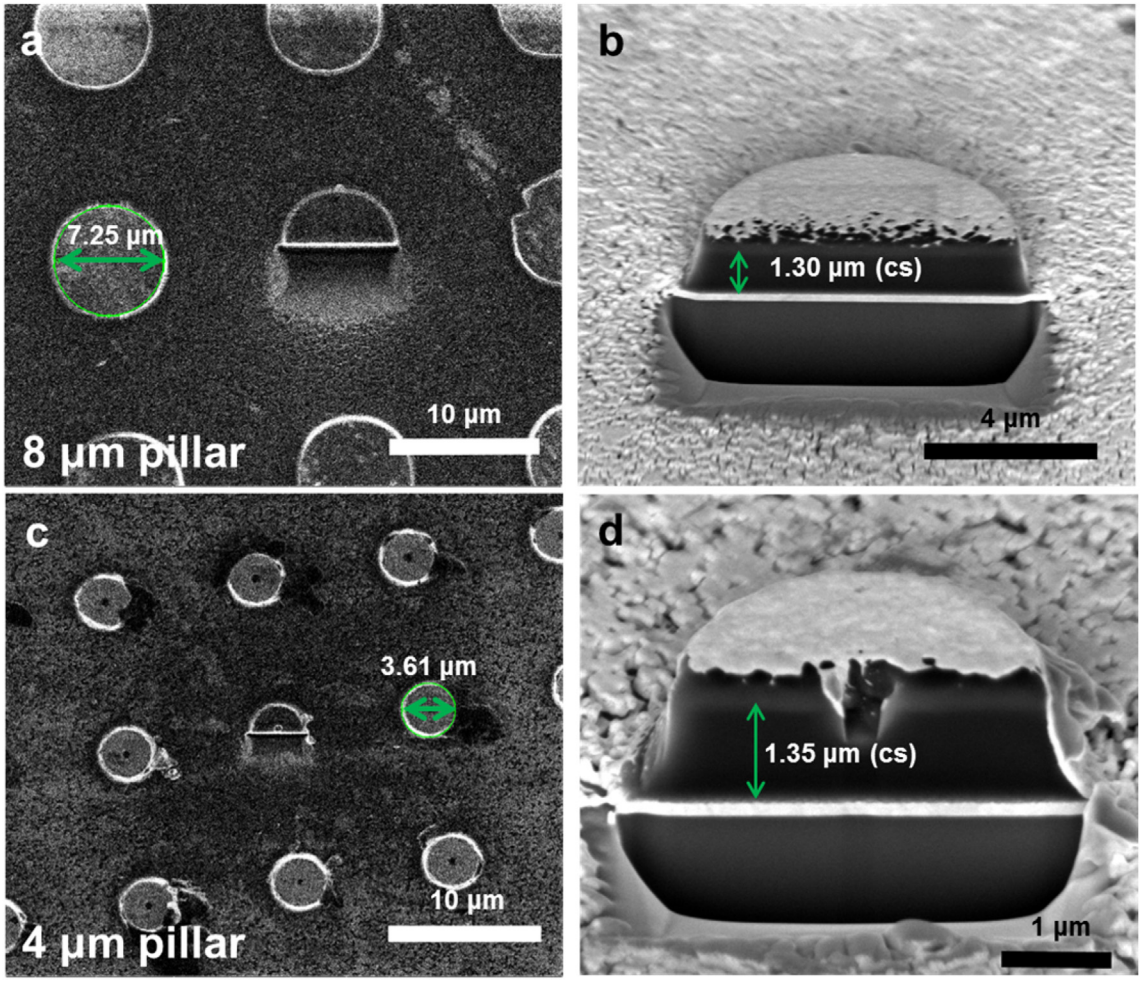

Fig. 1. FESEM images of the bare gold cylindrical pillars electrode with 8 μm and 4 μm diameter pillars. (a, c) Top view, 3500× magnification at 30 KV; (b, d) Cross-section showing the height of the pillar on the electrode, tilted 52° at 5 kV at 10000x and 25000× of magnification, respectively.

VSP multichannel potentiostat (Bio-Logic, France). The electrochemical cells were operated at 23.0 ± 0.5 °C under constant stirring with a magnetic stirrer. Each condition was tested with at least two independent biological replicates (n = 2). The WEs are the microstructured electrodes described in Section 2.1: 8 μm (a) and 4 μm (b) cylindrical pillar arrays and flat electrode (c) without any microstructure. The WEs were characterized at the beginning (following inoculation) and the end of the experiments through cyclic voltammetry (CV) (Supplementary Fig. S3) and electrochemical impedance spectroscopy (EIS), which was performed at open circuit potential (OCP) without stirring. The EIS was carried out in the frequency range 100 KHz-30 mHz. The AC potential amplitude was 10 mV. The full set of EIS parameters (.MPS file) is included as supplementary information. Charge output was measured at 400 mV vs. Ag/AgCl through Chronocoulometry (CC) under stirring conditions. EIS results were fitted to the equivalent circuit model through the EC-Lab software v11.26 (Bio-Logic, France).

2.4. Imaging of E. coli attachment onto the electrode

At the end of the electrochemical characterization, all the electrodes were imaged through CLSM or FESEM to determine the effect of electrode microstructure on biofilm formation. The electrodes were removed from the electrochemical cells and rinsed with phosphate buffered saline (PBS) to remove the planktonic cells. For FESEM imaging, the biointerface was dehydrated with ethanol at increasing concentrations (25%, 50% 75%, and 100%). Then, the electrode was placed in glutaraldehyde 3% at 5 °C for 24 h for fixation on the surface and then dried at room temperature. Finally, the electrode was coated with platinum (Pt) for FESEM observation.

After the removal of the planktonic cells with PBS, the electrodes were stained with a mixture of fluorescent dyes LIVE/DEAD™ BacLight™ Bacterial Viability Kit to image separately viable and dead cells attached on the surface of the electrode. The dyes (SYTO® 9 and propidium iodide) were mixed in equal part and deposited on the electrodes for 15 min. The electrode was then rinsed with PBS to eliminate the excess of dye and then imaged with a 40× magnification CLSM (Zeiss 5780 microscope (Zeiss, Germany)). The reflection technique was used to visualize the metal surface [41].

2.5. Statistical analysis

All the electrodes were fabricated in one batch on the same 10″ silicon wafer. Later, the electrodes were cut, randomized, and used for the bioelectrochemistry experiments. Each experiment was inoculated with independent overnight cultures of *E. coli*. Each chronocoulometric (CC) curve, discussed in section 3.1, is the average of four independent biological replicates (N = 4). All the EIS results, discussed in section 3.2, are calculated from two independent biological replicates (N = 2). Average and standard deviation of the results were calculated using standard methods.

3. Results and discussion

3.1. Effect of microstructure electrodes on the EET process

The potentiostat-controlled electrochemical cells were inoculated with overnight grown *E. coli* culture to a final $OD_{600} = 0.7$, which corresponds to fully grown *E. coli* culture in MOPS [42]. Following inoculum, the bacterial cell concentration in the planktonic phase remained approximately constant during the experiments. Therefore, the difference in the charge output across the Au electrode microstructures tested originated mainly from the bacterial attachment and initial biofilm formation during the 24 h of the batch experiments. This experimental setup consents deconvoluting the effect of bacterial growth in the planktonic phase from the biofilm growth. In previously reported experiments, in fact, the change on current output with time was the combined effect of growth in planktonic phase and early biofilm formation [43–45].

Three types of electrodes: cylindrical pillars ordered arrays of 8 μm, and 4 μm in diameter, and smooth flat electrode (without microstructure) were tested in potentiostat-controlled electrochemical cells. The working electrodes were maintained at E = 0.4 V vs. Ag/AgCl, which is higher than the limiting potential for 2-HNQ but not too high to damage the bacterial membranes and the EET chain [46,47]. The charge output over 24 h was calculated from the current output via numerical integration using EC-Lab software. Previous experiments show that 24 h at 37 °C gives enough time to observe *E. coli* biofilm formation in flow cells [48]. Under batch conditions, longer experiments could not be performed, as the nutrients are rapidly consumed, leading to a strong decrease in the current output. Longer experiments (36 h) in continuous flow cells at 30 °C have been previously reported, showing complete biofilm formation under these conditions [49], with 70–100 μm thick colonies. However, thick biofilms (multilayers biofilm) with full surface coverage hinder the effect of electrode microstructure on EET [30,50], thus short experiments at lower temperature are preferable to study the effect of microstructure on EET in biofilms.

The charge output at 24 h of the 8 μm and 4 μm pillars microstructured electrodes was 22% and 11% higher than that of the flat electrodes (Fig. 2). The electrodes with 8 μm, 4 μm cylindrical pillars and the flat electrodes produced 0.299 ± 0.018C, 0.273 ± 0.028C and 0.244 ± 0.021C per cm^2 of geometric surface after 24 h, respectively (n = 4). The electrodes have a surface area of 0.30 (flat electrode), 0.31 (4 μm pillars), and 0.32 cm^2 (8 μm pillars). The physical increment of the geometric area corresponds to 3% and 6% for 4 and 8 μm pillars microstructure electrodes, respectively. Surprisingly, the effectiveness is 3.66 times higher for the charge output as calculated by surface increased (22% and 11% more charge). This result suggests that the charge output increases mainly due to the formation of biofilm, and not only to the redox cycling of 2-HNQ mediated by the suspended cells in the planktonic phase, which is proportional to the geometric surface of the

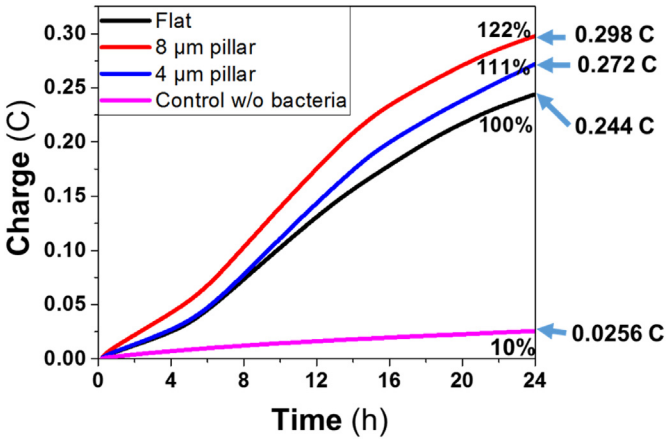

Fig. 2. Charge-time response measured for the 8 μm (red line), 4 μm (blue line) pillars and flat electrode (black line) with a potential step of 0.4 V versus Ag/AgCl over 24 h. The solution included MOPs buffer, *E. coli* at $OD_{600} = 0.7$, and 50 μM of 2-HNQ as redox mediator. Control experiment with flat electrode without bacteria (pink line) bacteria is included. Each line represents the average of four independent biological replicates (n = 4) with new electrodes and overnight-grown bacteria.

electrode. However, direct quantification of planktonic and biofilm cells through flow cytometry or colony forming units (CFU) might be needed to confirm the validity of our results. We have recently observed that the concentration of planktonic cells does not change significantly in 24 h of *E. coli* biofilm growth [24], thus indicating that charge transfer is contributed mostly by the biofilms, under the chosen experimental conditions. The effect of a small increment of the geometric surface area on the charge output in *E. coli* has not been reported. Notably, the correlation between electrode surface area and charge output is nonlinear. For example, an increment of 573% of geometric area correspond to a 236% increase in current for *Geobacter sulfurreducens*, which in turn corresponds to only 40% of surface area increase [30]. This result is relevant to determine the optimal surface area for detection of initial biofilm formation in biomedical devices.

Each CC curve (Fig. 2) represents the average of four independent biological replicates (n = 4). The charge output variability results in partial overlapping of the 8 μm and 4 μm pillars microstructured electrodes. The charge output variability can be explained by the colonization patterns (isolated cells to patches), and the stochastic nature of initial biofilm attachment [30,51], due to the reversible attachment/detachment phenomena. The charge output is comparable with that of other weak electroactive microorganisms such as *Enterococcus faecalis* [52] in presence of 0.5 mM concentration of Fe(II)/Fe(III) as redox mediator. Sterile control experiments with flat Au electrodes produce less than 10% of the experiments inoculated with viable cells, confirming that the current output is caused by the reduction of 2-HNQ by metabolically active viable cells and its re-oxidation at the electrode maintained at oxidizing potential (Fig. 2).

The charge output with time follows similar trend for microstructured and flat electrodes. After inoculation, the charge increases gradually in the first 5 h, which is followed by a rapid increase. Interestingly, this increase did not follow a logarithmic trend (Supplementary Fig. S3), indicating that the charge production was not related to bacterial duplication in planktonic phase but rather to bacterial biofilm formation [43]. After 15 h, the charge output rate decreased, probably due to nutrient limitations. Previous reports have suggested that the charge output plateau is due to limitation in EET through thick biofilms [30,53]. The plateau in charge production has been previously observed for growing bacterial culture, and it is not yet clear whether this is due to exhaustion of nutrients or excessive accumulation of biofilm, which decreases biofilm conductivity and charge output rate. In this system, charge output plateau might also be caused by coverage of surface microstructure. However, the same effect was observed for flat electrodes, suggesting that charge plateau is mostly due to the nutrient exhaustion. Further, the CLSM analysis (discussed in section 3.3) shows only partial coverage on the electrode, thus the nutrient limitation explanation is more likely. The CV analysis (Supplemental Fig. 4) shows a poorly reversible oxidation peak at 0.05 V vs. Ag/AgCl after biofilm formation (24 h). The height of the peak is higher for microstructured than flat electrodes. However, no significant difference between 4 and 8 μm was observed.

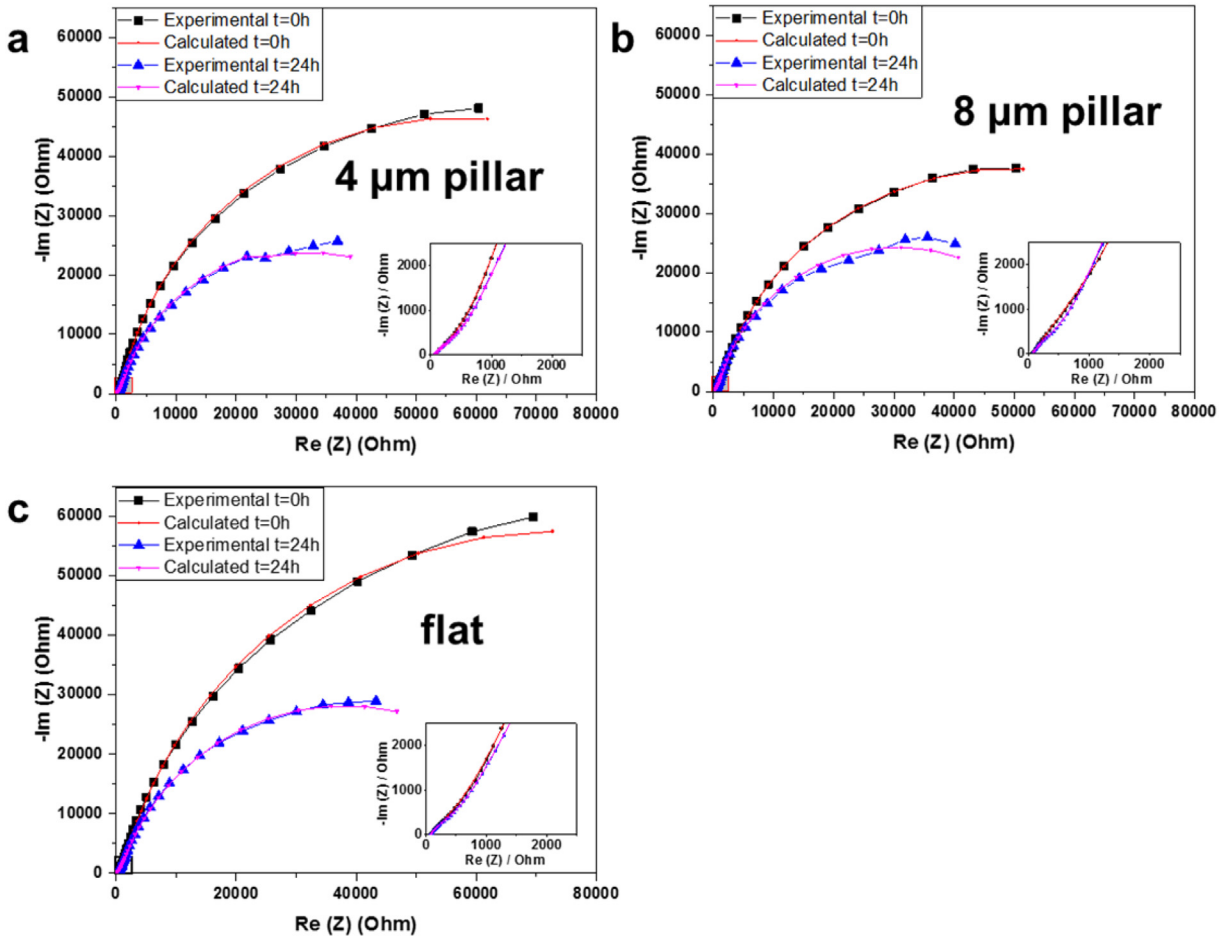

Fig. 3. Nyquist plot of EIS response and fitting to the equivalent circuit model, for (a) 4 μm pillars, (b) 8 μm pillars, and (**c**) control flat electrode, before (0 h) and after biofilm formation (24 h). Insets show the high frequency portion of the EIS scan. Each experiment was repeated with two independent biological replicates (n = 2).

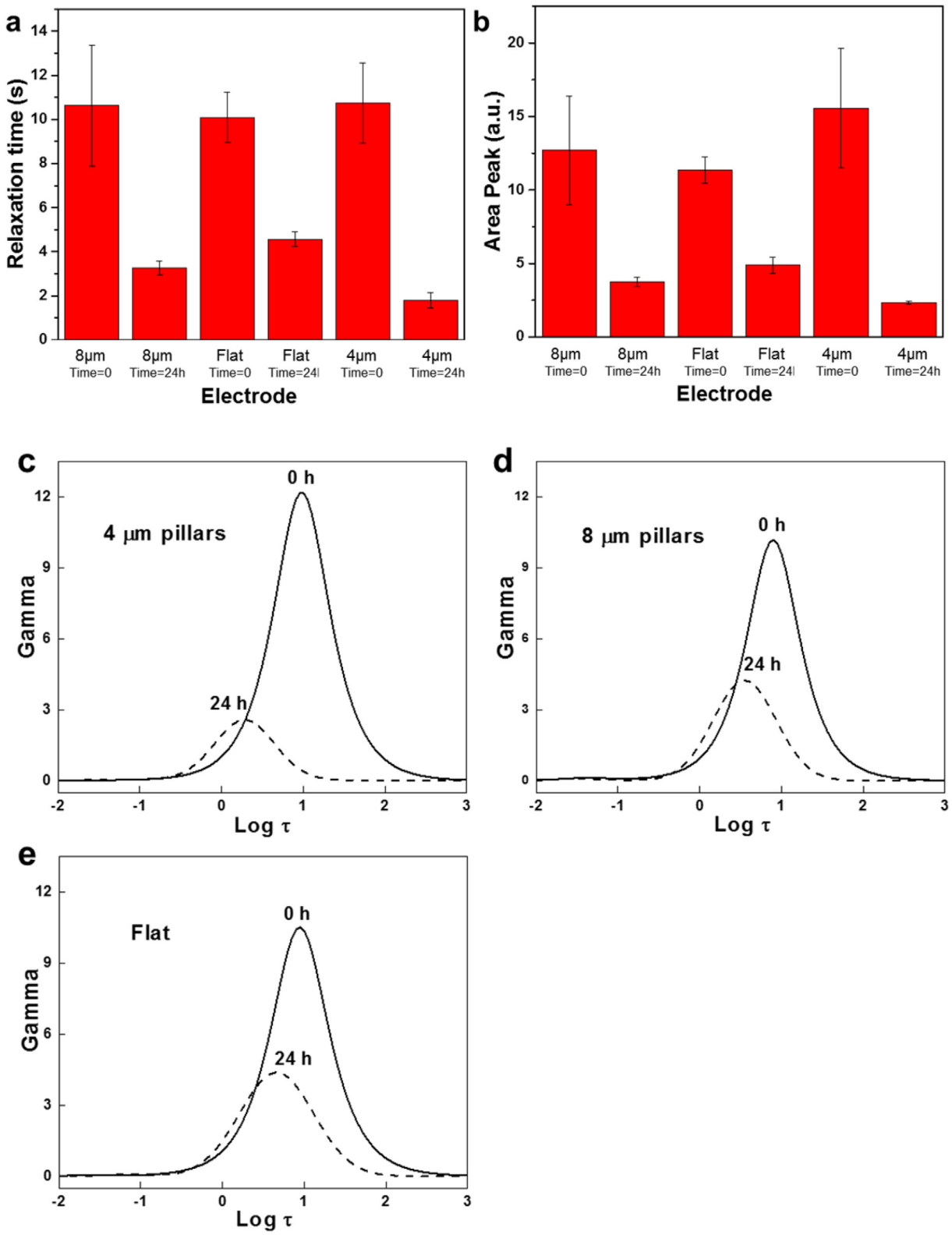

Fig. 4. (**a**) Relaxation time (τ) and (b) gamma main-peak area value from electrochemical impedance spectroscopy (EIS) before (t = 0 h) and after biofilm formation (t = 24 h), using ordered structure array gold electrodes of 4 μm and 8 μm pillars, and flat electrodes; (c–e) Gamma as function of relaxation time (Log τ) for the 4 μm and 8 μm microstructure and flat electrodes. The reduction and left-displacement of the peak areas after biofilm formation (t = 24 h, dashed lines) correspond to a decrease of the impedance and to acceleration of EET at the biofilm-electrode interface.

3.2. Early biofilm attachment on the electrode surface impedance

The Nyquist plot for the smooth and microstructured electrodes (8 μm and 4 μm diameter cylindrical pillars) immediately after inoculation (time = 0 h) and at 24 h is shown in Fig. 3. The EIS show features at high frequency (HF) and low frequency (LF). While the HF feature does not change with biofilm formation, the impedance at LF decreases significantly with time as early biofilm attaches onto the electrode. It has been previously shown that *E. coli* does not produce a current output without a redox mediator [1,36]. Thus, the EIS feature at LF is due to the following processes: 1. Molecular diffusion of 2-HNQ from bulk solution to the biofilm; 2. Reduction of 2-HNQ in the biofilm; 3. Re-oxidation of 2-HNQ at the electrode polarized at high potential. The EIS feature at HF is likely due to the impedance of the electrode-charge collector connection, which is much smaller than that at LF. Prior to equivalent circuit modeling of the EIS result, the distribution function of relaxation times (DFRT) was obtained using the software ISGP [54,55] to determine the number of time constants in the system and their variation with biofilm growth. The raw EIS data were trimmed to remove the noise caused by the electrode connection (HF) and the diffusional limitations (LF), thus isolating the time constants of the system. The gamma function, corresponding to the total impedance of the RC circuit associated to each time constant, and the characteristic time for the RC circuit decreases with time for all electrodes (Fig. 4), indicating a more efficient EET process as biofilm forms on the electrode. This is due to the faster redox cycling of 2-HNQ in presence of biofilms, as per the EET process previously discussed. The relaxation time decreases from 10 s to 5 s approximately after biofilm formation. However, no significant difference in the relaxation time was observed between electrodes of different microstructure. Similarly, the decreases of gamma function after biofilm growth does not show statistical difference across the microstructure. The DFRT results confirm that the EIS data should be modeled with two times constant model, in which only the time constant at LF depends on biofilm formation.

The two time constants shown in the equivalent circuit of the system was used to fit the EIS data described by Eqs. (1) and (2) [56] (Supplementary Fig. S5):

$$Z(\omega) = R_1 + \frac{1}{(i\omega)^{\alpha_2} Q_2 + \frac{1}{R_2}} + \frac{1}{(i\omega)^{\alpha_3} Q_3 + \frac{1}{R_3}} = R_1 + \frac{R_2}{1 + (i\omega)^{\alpha_2}\tau_2} + \frac{R_3}{1 + (i\omega)^{\alpha_3}\tau_3} \tag{1}$$

$$\tau_1 = R_1 Q_1,\ \tau_2 = R_2 Q_2 \tag{2}$$

where R_1 represents the ohmic resistance of the bulk solution in the cell. Q_3 is the constant phase element (CPE) that describes the pseudo-capacitance of the solution – biofilm interface and R_3 represent the resistance to charge transfer at the same interface. Q_2 and R_2 represented the biofilm – electrode interface in series with the solution-biofilm interface. Finally, α_2 and α_3 represent the nonideality of pseudo-capacitance Q_2 and Q_3, respectively. Q_2 and R_2 are shown in the Supplementary Fig. S6.

The EIS results confirm that the microstructured electrodes improve the EET rate and the biofilm attachment in comparison with

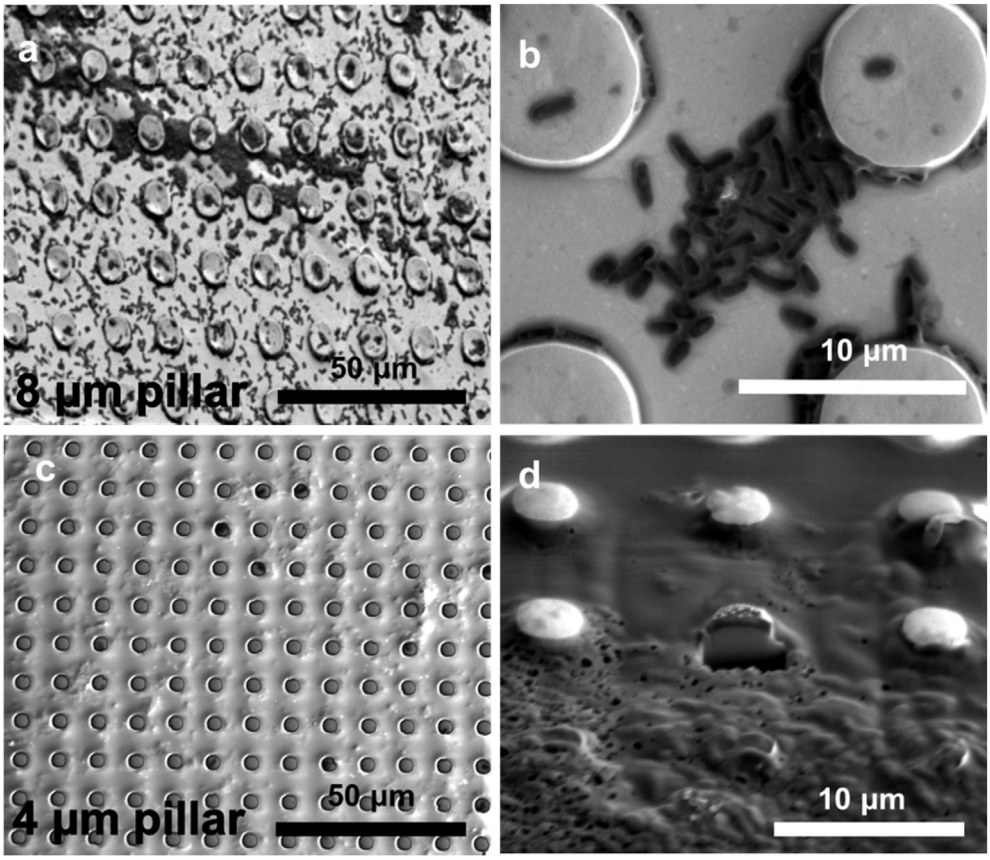

Fig. 5. FESEM images of the ordered structure array gold electrodes with bacteria attached onto their surface after 24 h of growth at 0.4 V vs. Ag/AgCl. (a) 8 μm pillars electrode top view, magnification 999×, 5 KV; (b) 8 μm pillars electrode top view, magnification 6000×, 5 KV; (c) 4 μm pillars electrode top view, magnification 1000×, 5 KV; (d) 4 μm pillars electrode tilted 52°, magnification 5000×, 5 KV.

the control flat electrode. The 8 μm pillar microstructure shows a slightly lower impedance, which corresponds to the lowest R_2 and highest Q_2 values (Supplementary Table S1). These results are consistent with previous observation of EET in *G. sulfurreducens* biofilms [15]. R_3 and Q_3 did not show a well-defined trend, as they do not depend on biofilm formation. Overall, the EIS at open circuit potential may be insufficient to determine the biofilm electrochemical signature. We therefore suggest that EIS at different potentials is routinely adopted for biofilm characterization, as recently reported [24], when faradaic current is sufficiently low not to alter the EIS results [57].

3.3. *Electrode morphology and biofilm-surface interaction imaging: FESEM and CLSM*

The distribution of the attached cell onto the electrode support the results of the electrochemical characterization of the biofilm-electrode interface. The microstructured electrodes were imaged before inoculation (0 h) and after early biofilm attachment (24 h). Flat electrodes images were not included.

FESEM of the bare electrode confirms the fabrication morphology in concordance with the designed characteristics. Fig. 1 shows the pillars array with smooth Au thin film deposited on the microstructures. The microstructures are homogeneously distributed with centers equally distant of 20 μm. The distance measured from the edge of the structure to the next one was 16 μm and 12 μm for the 4 μm and 8 μm, respectively, which is consistent with the lithography design. The 1 μm height of the pillar structure is smaller than previously reported microstructure, e.g., 500 μm height pillar [30], 8 μm height pillar [58], and 20 μm height pillar [34]. Higher pillars increase the geometrical surface area; however, they also increase diffusional limitations of the nutrient toward the biofilm. The optimal size of microstructure can vary depending on

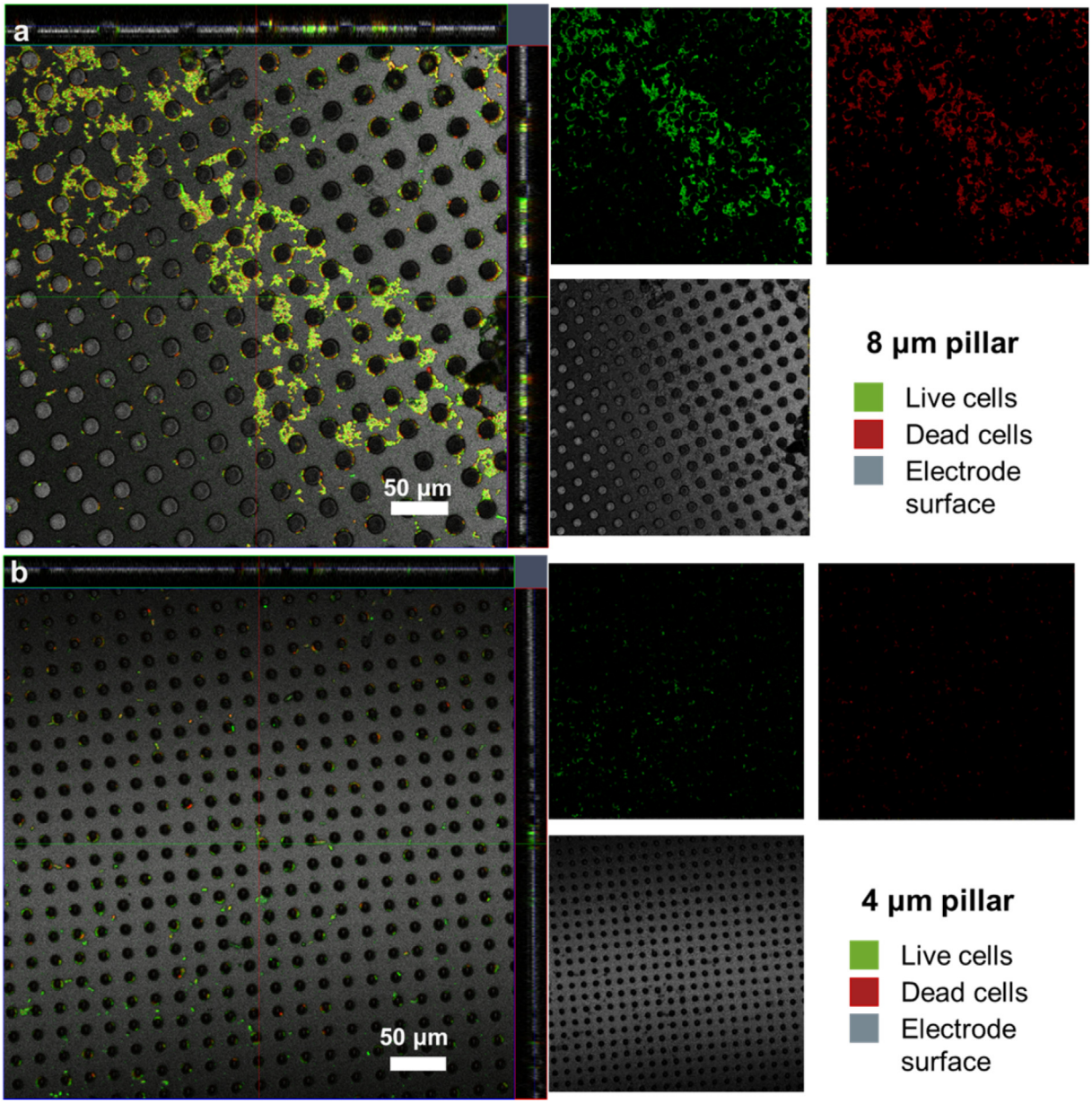

Fig. 6. CLSM images of the ordered structure array gold electrodes of (**a**) 8 μm and (**b**) 4 μm pillars, with bacteria attached onto their surface after 24 h of potential-controlled (0.4 V) electrochemical batch. SYTO® 9 and propidium iodide staining used to differentiate live and dead cells. Right-side panels display the individual channels for live cells, dead cells, and electrode surface.

the microorganisms used and the characteristics of the biofilm.

After 24 h, the early biofilm formed by *E. coli* was observed through FESEM and CLSM. The electrode was suspended vertically in the growth medium, to minimize bacterial deposition due to gravity and rinsed with PBS to remove planktonic cells and poorly attached cells from the electrode surface. The FESEM images showed different pattern of biofilm formation on the two microstructured electrodes, with higher surface coverage for the 8 μm pillars (Fig. 5(a) and b). The bacteria accumulate especially at the foot of the cylindrical pillars. The 4 μm pillars microstructured electrodes barely showed any biofilm accumulation. (Fig. 5(c)). However, bacteria were visible on the tilted image as rod-shaped object (Fig. 5(d)). FESEM images do not allow identifying biofilm matrix, thus further experiments with biofilm-specific dyes are needed. A cross-section performed with focused ion beam system (FIB) showed the biological layer covering the electrode had a thickness of approximately 500 nm which is consistent with the thickness of *E. coli* monolayer.

The FESEM results were confirmed by CLSM images. In fact, the distance between features appear to affect biofilm formation, with higher biofilm growth for 12 μm distance than 16 μm, as shown in Fig. 6. As in FESEM images, most bacteria were observed as small aggregates at the foot of pillars. Previous results show preference of bacteria for micropatterned surface at initial attachment [59] and for the grain boundaries of stainless steel [60]. The biomass of the biofilm grown on the 8 μm pillar electrodes was $6.3 \pm 2.1\ \mu m^3$ for viable and $8.9 \pm 3.6\ \mu m^3$ for dead cells, respectively, resulting in a biofilm thickness of 0.40 μm (Fig. 6(a)). In the case of the 4 μm pillar electrodes, the CLSM showed a live cells biomass of $4{,}3 \pm 0.7\ \mu m^3$ and dead cells biomass of $3.4 \pm 0.8\ \mu m^3$ leading to a biofilm thickness of 0.34 μm (Fig. 6(b)). Both the viable biomass and the biofilm thickness were lower for the 4 μm than for the 8 μm electrodes, which is consistent with the lower current output observed. Overall, the FESEM and CLSM results support the electrochemical data, suggesting that the microstructures on the electrode favor the attachment of the early biofilm onto the electrode, hence the EET is affected as well. Interestingly, the significant difference in biofilm formation among different microstructure does not correlate with the small difference in surface area, indicating that the spatial arrangement of microstructures influences early biofilm formation, rather than the overall surface area of the electrodes.

4. Conclusion

Electron transfer rate between viable *E. coli* biofilms and gold thin films was measured on flat and microstructured ordered array electrodes poised at oxidative potential. The effect of bacterial growth on EET rate was deconvoluted from the biofilm formation, showing that EET depends on the initial biofilm attachment, which in turn depends on the electrode microstructure. Bacterial attachment and initial biofilm formation were visually confirmed via FESEM and CLSM imaging, while the decrease of interfacial impedance following biofilm formation was experimentally measured through EIS, and then fitted to a two times constant model. Microstructured electrodes enhanced the charge output and helped understand the details of the bacteria-surface interactions in early biofilm formation. Rapid detection of early or residual biofilms through microstructured surfaces with well-defined roughness and aspect ratio is a desirable feature in biomedical devices and drinking water systems. Surface and aspect ratio design of such microstructures can be customized for each specific application. Future research efforts should focus on conductive ceramics and conductive polymers, which are commonly adopted in dental coatings and food/packaging industry.

Conflicts of interest

The authors declare no competing interests.

Data availability

The raw/processed data required to reproduce these findings are available from the authors upon request.

Declaration of competing interest

The authors declare that they have no known competing financial interests or personal relationships that could have appeared to influence the work reported in this paper.

CRediT authorship contribution statement

Solange E. Astorga: Conceptualization, Writing - original draft, Writing - review & editing. **Liang Xing Hu:** Writing - review & editing. **Enrico Marsili:** Conceptualization, Writing - original draft, Writing - review & editing. **Yizhong Huang:** Conceptualization, Writing - review & editing.

Acknowledgements

We thank Abeed Mohidin-Batcha for assistance inoculating bacteria, Prasanna Jogdeo for assistance with CLSM imaging, Cao Xun for assistance with FESEM imaging, and Ezequiel Santillan for revising the manuscript.

This work was supported by Singapore Centre for Environmental Life Sciences Engineering (SCELSE), whose research is supported by the National Research Foundation Singapore, Ministry of Education, Nanyang Technological University and National University of Singapore, under its Research Centre of Excellence Program. Additional support was provided by Material Science and Engineering, Nanyang Technological University, Tier 1 by the National Research Foundation Singapore, Ministry of Education (MOE) [M4011959 and M4011528]. Solange Elizabeth Astorga was partially supported by a Roberto Rocca fellowship.

Appendix A. Supplementary data

Supplementary data to this article can be found online at https://doi.org/10.1016/j.matdes.2019.108256.

References

[1] C. Santoro, C. Arbizzani, B. Erable, I. Ieropoulos, Microbial fuel cells: from fundamentals to applications. A review, J. Power Sources 356 (2017) 225–244.
[2] K. Rabaey, J. Rodriguez, L.L. Blackall, J. Keller, P. Gross, D. Batstone, W. Verstraete, K.H. Nealson, Microbial ecology meets electrochemistry: electricity-driven and driving communities, ISME J. 1 (1) (2007) 9–18.
[3] K.P. Katuri, S. Kalathil, A.a. Ragab, B. Bian, M.F. Alqahtani, D. Pant, P.E. Saikaly, Dual-function electrocatalytic and macroporous hollow-fiber cathode for converting waste streams to valuable resources using microbial electrochemical systems, Adv. Mater. 30 (26) (2018) 1707072.
[4] B.E. Logan, M. Elimelech, Membrane-based processes for sustainable power generation using water, Nature 488 (7411) (2012) 313.
[5] H.D. Beyene, A.A. Werkneh, T.G. Ambaye, Current updates on waste to energy (WtE) technologies: a review, Renew. Energy Focus 24 (2018) 1–11.
[6] B.E. Logan, Exoelectrogenic bacteria that power microbial fuel cells, Nat. Rev. Microbiol. 7 (5) (2009) 375–381.
[7] J.A. Gralnick, D.K. Newman, Extracellular respiration, Mol. Microbiol. 65 (1) (2007) 1–11.
[8] A.J. Stams, F.A. De Bok, C.M. Plugge, V. Eekert, H. Miriam, J. Dolfing, G. Schraa, Exocellular electron transfer in anaerobic microbial communities, Environ. Microbiol. 8 (3) (2006) 371–382.
[9] C.R. Myers, J.M. Myers, Localization of cytochromes to the outer membrane of anaerobically grown Shewanella putrefaciens MR-1, J. Bacteriol. 174 (11) (1992) 3429–3438.

[10] D. Prasad, S. Arun, M. Murugesan, S. Padmanaban, R. Satyanarayanan, S. Berchmans, V. Yegnaraman, Direct electron transfer with yeast cells and construction of a mediatorless microbial fuel cell, Biosens. Bioelectron. 22 (11) (2007) 2604–2610.
[11] Y.A. Gorby, S. Yanina, J.S. McLean, K.M. Rosso, D. Moyles, A. Dohnalkova, T.J. Beveridge, I.S. Chang, B.H. Kim, K.S. Kim, Electrically conductive bacterial nanowires produced by Shewanella oneidensis strain MR-1 and other microorganisms, Proc. Natl. Acad. Sci. 103 (30) (2006) 11358–11363.
[12] G. Reguera, K.D. McCarthy, T. Mehta, J.S. Nicoll, M.T. Tuominen, D.R. Lovley, Extracellular electron transfer via microbial nanowires, Nature 435 (7045) (2005) 1098.
[13] B.E. Logan, J.M. Regan, Electricity-producing bacterial communities in microbial fuel cells, Trends Microbiol. 14 (12) (2006) 512–518.
[14] K. Rabaey, N. Boon, M. Höfte, W. Verstraete, Microbial phenazine production enhances electron transfer in biofuel cells, Environ. Sci. Technol. 39 (9) (2005) 3401–3408.
[15] J.T. Babauta, H. Beyenal, Use of a small overpotential approximation to analyze Geobacter sulfurreducens biofilm impedance, J. Power Sources 356 (2017) 549–555.
[16] H.-C. Flemming, J. Wingender, The biofilm matrix, Nat. Rev. Microbiol. 8 (9) (2010) 623.
[17] J. Babauta, R. Renslow, Z. Lewandowski, H. Beyenal, Electrochemically active biofilms: facts and fiction. A review, Biofouling 28 (8) (2012) 789–812.
[18] E. Marsili, J.B. Rollefson, D.B. Baron, R.M. Hozalski, D.R. Bond, Microbial biofilm voltammetry: direct electrochemical characterization of catalytic electrode-attached biofilms, Appl. Environ. Microbiol. 74 (23) (2008) 7329–7337.
[19] J. Arnold, G. Bailey, Surface finishes on stainless steel reduce bacterial attachment and early biofilm formation: scanning electron and atomic force microscopy study, Poult. Sci. 79 (12) (2000) 1839–1845.
[20] K.D. Esmeryan, I.A. Avramova, C.E. Castano, I.A. Ivanova, R. Mohammadi, E.I. Radeva, D.S. Stoyanova, T.G. Vladkova, Early stage anti-bioadhesion behavior of superhydrophobic soot based coatings towards Pseudomonas putida, Mater. Des. 160 (2018) 395–404.
[21] A. Susarrey-Arce, J.F. Hernández-Sánchez, M. Marcello, Y. Diaz-Fernandez, A. Oknianska, I. Sorzabal-Bellido, R. Tiggelaar, D. Lohse, H. Gardeniers, J. Snoeijer, Bacterial footprints in elastic pillared microstructures, ACS Appl. Bio Mater. 1 (5) (2018) 1294–1300.
[22] J. Hasan, S. Jain, R. Padmarajan, S. Purighalla, V.K. Sambandamurthy, K. Chatterjee, Multi-scale surface topography to minimize adherence and viability of nosocomial drug-resistant bacteria, Mater. Des. 140 (2018) 332–344.
[23] X. Li, T. Shi, B. Li, X. Chen, C. Zhang, Z. Guo, Q. Zhang, Subtractive manufacturing of stable hierarchical micro-nano structures on AA5052 sheet with enhanced water repellence and durable corrosion resistance, Mater. Des. 183 (2019) 108152.
[24] S.E. Astorga, L.X. Hu, E. Marsili, Y. Huang, Electrochemical signature of Escherichia coli on Ni micropillar array electrode for early biofilm characterization, ChemElectroChem (6) (2019) 4674–4680.
[25] Z. Jiao, Q. Wu, J. Qiu, Preparation and electrochemical performance of hollow activated carbon fiber-carbon nanotubes three-dimensional self-supported electrode for supercapacitor, Mater. Des. 154 (2018) 239–245.
[26] H. Beyenal, J.T. Babauta, Biofilms in Bioelectrochemical Systems: from Laboratory Practice to Data Interpretation, John Wiley & Sons, 2015.
[27] J. Gooding, W. Yang, The self-assembled monolayer modification of electrodes-some recent advances in biological application, L'Act. Chim. 320 (321) (2008) 85–89.
[28] D. Mandler, S. Kraus-Ophir, Self-assembled monolayers (SAMs) for electrochemical sensing, J. Solid State Electrochem. 15 (7–8) (2011) 1535.
[29] E. Parra, L. Lin, Microbial fuel cell based on electrode-exoelectrogenic bacteria interface, Micro Electro Mechanical Systems, in: 2009. MEMS 2009. IEEE 22nd International Conference on, IEEE, 2009, pp. 31–34.
[30] P. Champigneux, C. Renault-Sentenac, D. Bourrier, C. Rossi, M.-L. Delia, A. Bergel, Effect of surface nano/micro-structuring on the early formation of microbial anodes with Geobacter sulfurreducens: experimental and theoretical approaches, Bioelectrochemistry 121 (2018) 191–200.
[31] Z. Ye, M.W. Ellis, A.S. Nain, B. Behkam, Effect of electrode sub-micron surface feature size on current generation of Shewanella oneidensis in microbial fuel cells, J. Power Sources 347 (2017) 270–276.
[32] S. Inoue, E.A. Parra, A. Higa, Y. Jiang, P. Wang, C.R. Buie, J.D. Coates, L. Lin, Structural optimization of contact electrodes in microbial fuel cells for current density enhancements, Sens. Actuators A Phys. 177 (2012) 30–36.
[33] P. Champigneux, M.-L. Delia, A. Bergel, Impact of electrode micro-and nano-scale topography on the formation and performance of microbial electrodes, Biosens. Bioelectron. (2018).
[34] J. Kim, J. Hwan Ko, J. Lee, M. Jun Kim, D. Byun, Power enhancement of a μ l-scale microbial fuel cells by surface roughness, Appl. Phys. Lett. 104 (22) (2014) 223702.
[35] J. Paredes, S. Becerro, S. Arana, Label-free interdigitated microelectrode based biosensors for bacterial biofilm growth monitoring using Petri dishes, J. Microbiol. Methods 100 (2014) 77–83.
[36] J. Hinks, E.J. Han, V.B. Wang, T.W. Seviour, E. Marsili, J.S. Loo, S. Wuertz, Naphthoquinone glycosides for bioelectroanalytical enumeration of the faecal indicator Escherichia coli, Microbial Biotechnol. 9 (6) (2016) 746–757.
[37] W.A. Rutala, D.J. Weber, Guideline for Disinfection and Sterilization in Healthcare Facilities, vol. 2008, 2008.
[38] N. Alipour, A. Karagoz, A. Taner, N. Gaeini, N. Alipour, H. Zeytin, F. Yildiz, R. Durmaz, Outbreak of hospital infection from biofilm-embedded pan drug-resistant Pseudomonas aeroginosa, due to a contaminated bronchoscope, J. Prevent. Med. 2 (2) (2017).
[39] M. Carminati, L. Mezzera, G. Ferrari, M. Sampietro, A. Turolla, M. Di Mauro, M. Antonelli, A Smart Sensing Node for Pervasive Water Quality Monitoring with Anti-fouling self-diagnostics, in: 2018 IEEE Internatisonal Symposium on Circuits and Systems (ISCAS), IEEE, 2018, pp. 1–5.
[40] O. Laczka, J.-M. Maesa, N. Godino, J. del Campo, M. Fougt-Hansen, J.P. Kutter, D. Snakenborg, F.-X. Muñoz-Pascual, E. Baldrich, Improved bacteria detection by coupling magneto-immunocapture and amperometry at flow-channel microband electrodes, Biosens. Bioelectron. 26 (8) (2011) 3633–3640.
[41] T.R. Neu, J.R. Lawrence, Development and structure of microbial biofilms in river water studied by confocal laser scanning microscopy, FEMS (Fed. Eur. Microbiol. Soc.) Microbiol. Ecol. 24 (1) (1997) 11–25.
[42] F.C. Neidhardt, P.L. Bloch, D.F. Smith, Culture medium for enterobacteria, J. Bacteriol. 119 (3) (1974) 736–747.
[43] A.P. Borole, G. Reguera, B. Ringeisen, Z.-W. Wang, Y. Feng, B.H. Kim, Electroactive biofilms: current status and future research needs, Energy Environ. Sci. 4 (12) (2011) 4813–4834.
[44] I.A. Ieropoulos, J. Greenman, C. Melhuish, J. Hart, Comparative study of three types of microbial fuel cell, Enzym. Microb. Technol. 37 (2) (2005) 238–245.
[45] D.H. Park, J.G. Zeikus, Electricity generation in microbial fuel cells using neutral red as an electronophore, Appl. Environ. Microbiol. 66 (4) (2000) 1292–1297.
[46] T. Seviour, L.E. Doyle, S.J.L. Lauw, J. Hinks, S.A. Rice, V.J. Nesatyy, R.D. Webster, S. Kjelleberg, E. Marsili, Voltammetric profiling of redox-active metabolites expressed by Pseudomonas aeruginosa for diagnostic purposes, Chem. Commun. 51 (18) (2015) 3789–3792.
[47] M.A. TerAvest, L.T. Angenent, Oxidizing electrode potentials decrease current production and coulombic efficiency through cytochrome c inactivation in shewanella oneidensis MR-1, ChemElectroChem 1 (11) (2014) 2000–2006.
[48] T.K. Wood, A.F.G. Barrios, M. Herzberg, J. Lee, Motility influences biofilm architecture in Escherichia coli, Appl. Microbiol. Biotechnol. 72 (2) (2006) 361–367.
[49] A. Reisner, J.A. Haagensen, M.A. Schembri, E.L. Zechner, S. Molin, Development and maturation of Escherichia coli K-12 biofilms, Mol. Microbiol. 48 (4) (2003) 933–946.
[50] F. Zhang, X. Xia, Y. Luo, D. Sun, D.F. Call, B.E. Logan, Improving startup performance with carbon mesh anodes in separator electrode assembly microbial fuel cells, Bioresour. Technol. 133 (2013) 74–81.
[51] D.E. Moormeier, J.L. Bose, A.R. Horswill, K.W. Bayles, Temporal and stochastic control of Staphylococcus aureus biofilm development, mBio 5 (5) (2014) e01341-14.
[52] D. Keogh, L.N. Lam, L.E. Doyle, A. Matysik, S. Pavagadhi, S. Umashankar, P.M. Low, J.L. Dale, Y. Song, S.P. Ng, Extracellular electron transfer powers Enterococcus faecalis biofilm metabolism, mBio 9 (2) (2018) e00626-17.
[53] E. Marsili, D.B. Baron, I.D. Shikhare, D. Coursolle, J.A. Gralnick, D.R. Bond, Shewanella secretes flavins that mediate extracellular electron transfer, Proc. Natl. Acad. Sci. 105 (10) (2008) 3968–3973.
[54] S. Baltianski, Y. Tsur, Analyzing Impedance Spectroscopy Results, Rare Metal Materials and Engineering, 2006, p. S3.
[55] A. Tesler, D. Lewin, S. Baltianski, Y. Tsur, Analyzing results of impedance spectroscopy using novel evolutionary programming techniques, J. Electroceram. 24 (4) (2010) 245–260.
[56] J.P. Diard, B. Le Gorrec, C. Montella, Handbook of Electrochemical Impedance Spectroscopy, Bio-Logic, 2013.
[57] X. Dominguez-Benetton, S. Sevda, K. Vanbroekhoven, D. Pant, The accurate use of impedance analysis for the study of microbial electrochemical systems, Chem. Soc. Rev. 41 (21) (2012) 7228–7246.
[58] C.-P.-B. Siu, M. Chiao, A microfabricated PDMS microbial fuel cell, J. Microelectromech. Syst. 17 (6) (2008) 1329–1341.
[59] C. Díaz, P. Schilardi, R. Salvarezza, M.F.L. De Mele, Have flagella a preferred orientation during early stages of biofilm formation?: AFM study using patterned substrates, Colloids Surfaces B Biointerfaces 82 (2) (2011) 536–542.
[60] K.R. Sreekumari, K. Nandakumar, Y. Kikuchi, Bacterial attachment to stainless steel welds: significance of substratum microstructure, Biofouling 17 (4) (2001) 303–316.